Active-matter isomorphs in the size-polydisperse Ornstein-Uhlenbeck Lennard-Jones model

Daniel Jespersen, Lorenzo Costigliola, Jeppe C. Dyre,* and Shibu Saw†
Glass and Time, IMFUFA, Department of Science and Environment, Roskilde University, P.O. Box 260, DK-4000 Roskilde, Denmark
(Dated: May 18, 2023)

This paper studies size-polydisperse Lennard-Jones systems described by active Ornstein-Uhlenbeck particle dynamics. The focus is on the existence of isomorphs (curves of invariant structure and dynamics) in the model's three-dimensional phase diagram. First, the isomorphs are traced out from a single steady-state configuration by means of the configurational-temperature method [Saw *et al.*, Phys. Rev. E **107**, 024609 (2023)]. Good invariance of the structure (probed by the reduced-unit radial distribution function) and of the dynamics (probed by the mean-square displacement as a function of time) is demonstrated for three uniform-distribution polydispersities, 12%, 23%, and 29%. Comparing to active-matter isomorphs generated by the analytical direct-isomorph-check method, the latter give somewhat worse invariance of the structure but better invariance of the dynamics. We conclude that both methods can be used to quickly get an overview of the phase diagram of AOUP models involving a potential-energy function obeying the hidden-scale-invariance symmetry that generally required for isomorph theory to apply.

* dyre@ruc.dk
† shibus@ruc.dk

I. INTRODUCTION

Active matter involves particles that absorb energy from their environment and perform motion, which is continuously dissipated into heat. This kind of motion, which in contrast to standard Newtonian or Brownian dynamics breaks time-reversal invariance [1, 2], is relevant in particular for describing biological systems ranging from bacteria to flocking birds [3–10]. Many different approaches to the description of active matter exist, depending on whether point particles or particles with directional coordinates are considered and depending on the precise mechanism by which the particles autonomously perform mechanical work [5, 6, 8, 9, 11, 12]. In this paper we consider one of the simplest active-matter models, the active Ornstein-Uhlenbeck particle (AOUP) model. The AOUP model involves point particles subject to colored-noise Langevin dynamics [13–16].

In view of the variability of biological systems, one cannot always expect all particles to be identical, and recently polydispersity has come into focus in connection with active-matter models [17–20]. There is also currently great interest in passive polydisperse systems coming from, in particular, their use in SWAP-equilibrated supercooled liquids [21] in which context the question arises of how similar the dynamics of small and large particles are [22–24].

This paper studies the size-polydisperse AOUP Lennard-Jones (LJ) model. We recently demonstrated the existence of lines of approximately invariant structure and dynamics in the phase diagram of a binary LJ AOUP model; such lines are referred to as "active-matter isomorphs" [25–27]. Inspired by the fact that the introduction of polydispersity into ordinary "passive" Newtonian models does not affect the existence of isomorphs [28], the present paper investigates whether the existence of isomorphs also survives the introduction of polydispersity into the AOUP model. Note that, besides conceptually simplifying the AOUP phase diagram, the existence of isomorphs makes it possible to quickly establish an overview of it because only one point on each isomorph needs to be simulated.

II. THE AOUP EQUATION OF MOTION AND SIMULATION DETAILS

We consider a system of N particles in volume V and define the number density by $\rho \equiv N/V$. If the potential-energy function is denoted by $U(\mathbf{R})$ in which $\mathbf{R} \equiv (\mathbf{r}_1, ..., \mathbf{r}_N)$ is the vector of all particle coordinates, the AOUP equation of motion [13–16] is

$$\dot{\mathbf{R}} \,=\, \mu \mathbf{F}(\mathbf{R}) \,+\, \boldsymbol{\eta}(t)\,. \tag{1}$$

Here μ is the mobility, i.e., velocity over force, and the $3N$-dimensional force vector is given by $\mathbf{F}(\mathbf{R}) = -\nabla U(\mathbf{R})$. The noise vector $\boldsymbol{\eta}(t)$ is colored according to an Ornstein-Uhlenbeck process, i.e., it is a Gaussian stochastic process characterized by

$$\langle \eta_i^\alpha(t) \eta_j^\beta(t') \rangle \,=\, \delta_{ij}\delta_{\alpha\beta} \frac{D}{\tau}\, e^{-|t-t'|/\tau} \tag{2}$$

where i and j are particle indices, α and β are xyz spatial indices, and D and τ are constants of dimension length squared over time and time, respectively.

We are interested in how the physics is affected when the density is changed, specifically in determining whether approximately invariant physics can be obtained by adjusting D and τ with density (μ is regarded as a material constant). For a binary AOUP model this problem was studied in Ref. 26 that demonstrated how to change D and τ with density in order to achieve invariant structure and dynamics to a good approximation. The question is whether this is possible also for systems with a significant size polydispersity.

In the AOUP model "reduced" quantities are defined by using $l_0 = \rho^{-1/3}$ as the length unit and $t_0 = \tau$ as the time unit [26]. Reduced quantities are marked by a tilde. When we speak below about approximately invariant structure and dynamics, this refers to the use of this state-point-dependent unit system.

We studied a system of $N = 5000$ particles in three dimensions interacting by Lennard-Jones (LJ) pair potentials that between particles i and j are given by $v_{ij}(r) = 4\varepsilon\left[(r/\sigma_{ij})^{-12} - (r/\sigma_{ij})^{-6}\right]$ with $\sigma_{ij} = (\sigma_i + \sigma_j)/2$ and $\varepsilon_{ij} = 1.0$ (Lorentz-Berthelot mixing rule). The particles sizes σ_i are distributed according to a uniform distribution with average equal to unity. Following the standard in the literature, the polydispersity δ is defined by $\delta^2 = (\langle\sigma^2\rangle - \langle\sigma\rangle^2)/\langle\sigma\rangle^2$, which in our case reduces to $\delta^2 = \langle\sigma^2\rangle - 1$ because $\langle\sigma\rangle = 1$. For the uniform distribution δ cannot exceed $1/\sqrt{3} \cong 58\%$. The three polydispersities studied in the present paper are $\delta \cong 11.5\%$, 23.1%, and 28.9%, corresponding to the size ranges listed in Table I (for brevity these are henceforth reported as $\delta = 12\%$, 23%, and 29%). Note that the study entails substantially different particle sizes, with the ratio of largest to smallest particle volume equal to 27 in the 29% polydispersity case.

δ	σ range	$\sigma_{max}/\sigma_{min}$
12%	$0.80 - 1.20$	1.50
23%	$0.60 - 1.40$	2.33
29%	$0.50 - 1.50$	3.00

TABLE I. Values of the polydispersity δ, σ range, and the corresponding ratio between largest and smallest particle sizes for the three cases studied.

All simulations used a shifted-force cutoff [29] of the ij particle interaction at pair distance $r = 2.5\sigma_{ij}$ and the time step $\Delta t = \Delta\tilde{t}/(D\ \rho^{2/3})$ in which $\Delta\tilde{t} = 0.4$ [26]. The active-matter simulations were carried out on GPU cards using a home-made code while the MD simulations used RUMD [30].

III. STRUCTURE AND DYNAMICS ALONG AN ISOCHORE

Before discussing results for the variation of the structure and dynamics along active-matter isomorphs, we briefly present analogous results along an isochore, i.e., for state points of the same density. The purpose is to set the stage by illustrating that structure and dynamics do vary significantly throughout the (ρ, D, τ) AOUP phase diagram. Structure is studied by means of the average radial distribution function (RDF) denoted by $g(r)$. In Fig. 2(a) RDFs are shown along the $\rho = 0.85$ isochore in the $\delta = 29\%$ case, with values of D and τ taken from the $\delta = 29\%$ active-matter isomorph studied in the next section. Figure 2(b) shows the same data in reduced coordinates that in the present case simply results in a common scaling of the x-coordinate.

We find substantial structure variation along the isochore. The same applies for the mean-square displacement (MSD) as a function of the time t, $\langle \Delta r^2(t) \rangle$, which is plotted in (c) in a log-log plot in LJ units and in reduced units in (d). The short-time slope is two, reflecting the "ballistic" regime of the AOUP model, which is not present in ordinary Langevin dynamics [13–16] because it results from short-time noise correlations, resulting in an inertia-like persistence of the direction of motion. At long times the well-known diffusive behavior leading to unity slope is observed. We note that the dynamics varies significantly along the isochore, whether or not it is reported in reduced units.

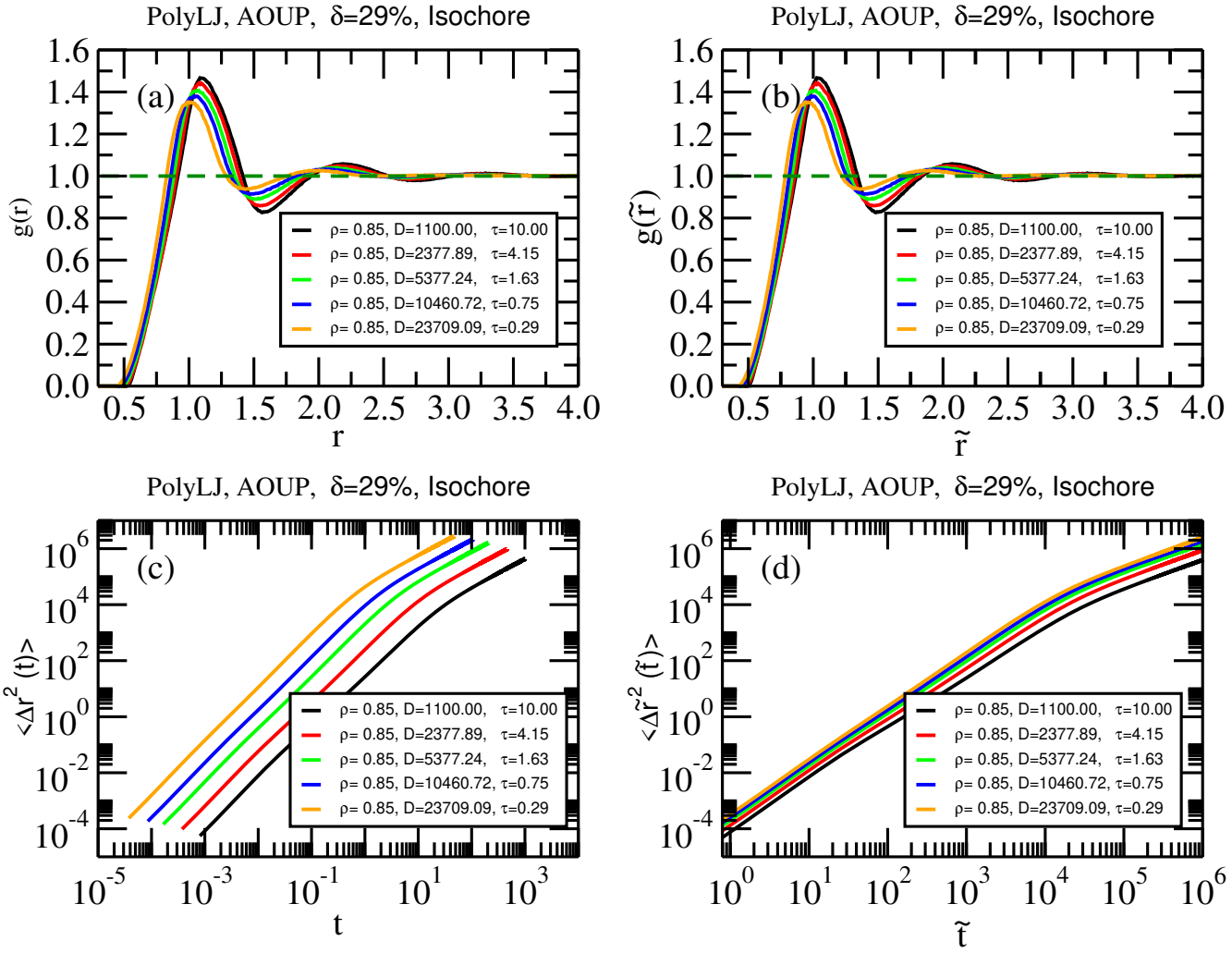

FIG. 1. Average radial distribution functions (RDF) as a function of the pair distance r and mean-square displacement (MSD) as a function of the time for state points on the $\rho = 0.85$ isochore of the $\delta = 29\%$ polydispersity LJ AOUP model (the D and τ values are those of the below studied $\delta = 29\%$ active-matter isomorph). (a) and (b) show the RDF as a function of r and the reduced pair distance $\tilde{r}$, respectively (the curves are the same because $\tilde{r} \propto r$ along an isochore). We see a substantial variation in the structure, with the most pronounced structure found for the smallest values of the model parameter D (black curves). The MSD likewise shows no collapse along the isochore, whether plotted (c) as a function of the time t or (d) as a function of the reduced time $\tilde{t}$. The slowest motion is found for the smallest D (black curves).

IV. STRUCTURE AND DYNAMICS ALONG $T_{\rm conf}$-GENERATED ACTIVE-MATTER ISOMORPHS

Reference 26 used the *configurational temperature* $T_{\rm conf}$ for determining how to change the AOUP model parameters D and τ with density in order to achieve approximately invariant reduced-unit structure and dynamics. The idea is that $k_BT_{\rm conf}$ is the relevant characteristic energy scale where $T_{\rm conf}$ is defined by $k_BT_{\rm conf} \equiv \langle(\nabla U)^2\rangle/\langle\nabla^2 U\rangle$ [31–33] in which k_B is the Boltzmann constant, ∇ is the gradient operator in the $3N$-dimensional configuration space, and the sharp brackets denote canonical-ensemble averages. In the thermodynamic limit the relative fluctuations of both the numerator and the denominator of $T_{\rm conf}$ go to zero, implying that it is enough to consider a single steady-state configuration using the expression $k_BT_{\rm conf} \cong (\nabla U(\mathbf{R}))^2/\nabla^2 U(\mathbf{R})$.

The reasoning of Ref. 26 may be summarized as follows. Adopting $e_0 = k_BT_{\rm conf}$ as the energy unit supplementing the above introduced length and time units ($l_0 = \rho^{-1/3}$; $t_0 = \tau$), we first note that the quantities $\mu t_0 e_0/l_0^2$, Dt_0/l_0^2, and τ/t_0 are dimensionless. Assuming that these three quantities cannot change with varying density if the structure and dynamics are invariant in reduced units, we conclude that $\mu \propto l_0^2/(t_0e_0) = \rho^{-2/3}/(\tau k_BT_{\rm conf})$ and $D \propto l_0^2/t_0 = \rho^{-2/3}/\tau$.

Since μ is assumed to be a material constant, this leads to $\tau \propto \rho^{-2/3}/k_B T_{\rm conf}$ and $D \propto k_B T_{\rm conf}$, i.e., to the following recipe for how D and τ changes with density in terms of their values D_0 and τ_0 at a reference state point of density ρ_0:

$$\begin{aligned} D(\rho) &= D_0 \, \frac{T_{\rm conf}(\rho)}{T_{\rm conf}(\rho_0)} \,, \\ \tau(\rho) &= \tau_0 \left(\frac{\rho_0}{\rho}\right)^{2/3} \frac{T_{\rm conf}(\rho_0)}{T_{\rm conf}(\rho)} \,. \end{aligned} \tag{3}$$

For a large system $T_{\rm conf}(\rho_0)$ may, as mentioned, be evaluated from a single configuration, which we denote by $\mathbf{R}_0$: $T_{\rm conf}(\rho_0) \cong T_{\rm conf}(\mathbf{R}_0)$. Ref. 26 demonstrated that this approximation introduces an negligible error for typical system sizes. In order to find $T_{\rm conf}(\rho)$ one scales $\mathbf{R}_0$ uniformly to the density ρ, i.e., substitute $\mathbf{R} = (\rho_0/\rho)^{1/3}\mathbf{R}_0$ into the configurational-temperature expression. This leads to

$$\begin{aligned} D(\rho) &= D_0 \, \frac{T_{\rm conf}\left[(\rho_0/\rho)^{1/3}\mathbf{R}_0\right]}{T_{\rm conf}(\mathbf{R}_0)} \,, \\ \tau(\rho) &= \tau_0 \left(\frac{\rho_0}{\rho}\right)^{2/3} \frac{T_{\rm conf}(\mathbf{R}_0)}{T_{\rm conf}\left((\rho_0/\rho)^{1/3}\mathbf{R}_0\right)} \,. \end{aligned} \tag{4}$$

We used these equations for generating three active-matter isomorphs starting in each case from the parameter values $D = 1100$ and $\tau = 10$ at the reference densities ρ_0 =0.99, 0.91, and 0.85, respectively, for the polydispersities $\delta = 12\%$, 23%, and 29% (these reference densities were chosen to have the same virial, i.e., the contributions to the pressure coming from interactions).

Results for the variation of the average RDF are given in Fig. 2. The left column reports the RDF of the three polydispersities as functions of the pair distance r, the right column shows the same data as functions of the reduced pair distance $\tilde{r}$. In the latter case we find a good, though not perfect data collapse, and conclude that the average structure is approximately invariant along the three active-matter isomorphs. This is not trivial in view of the fact that the density varies by a factor of two.

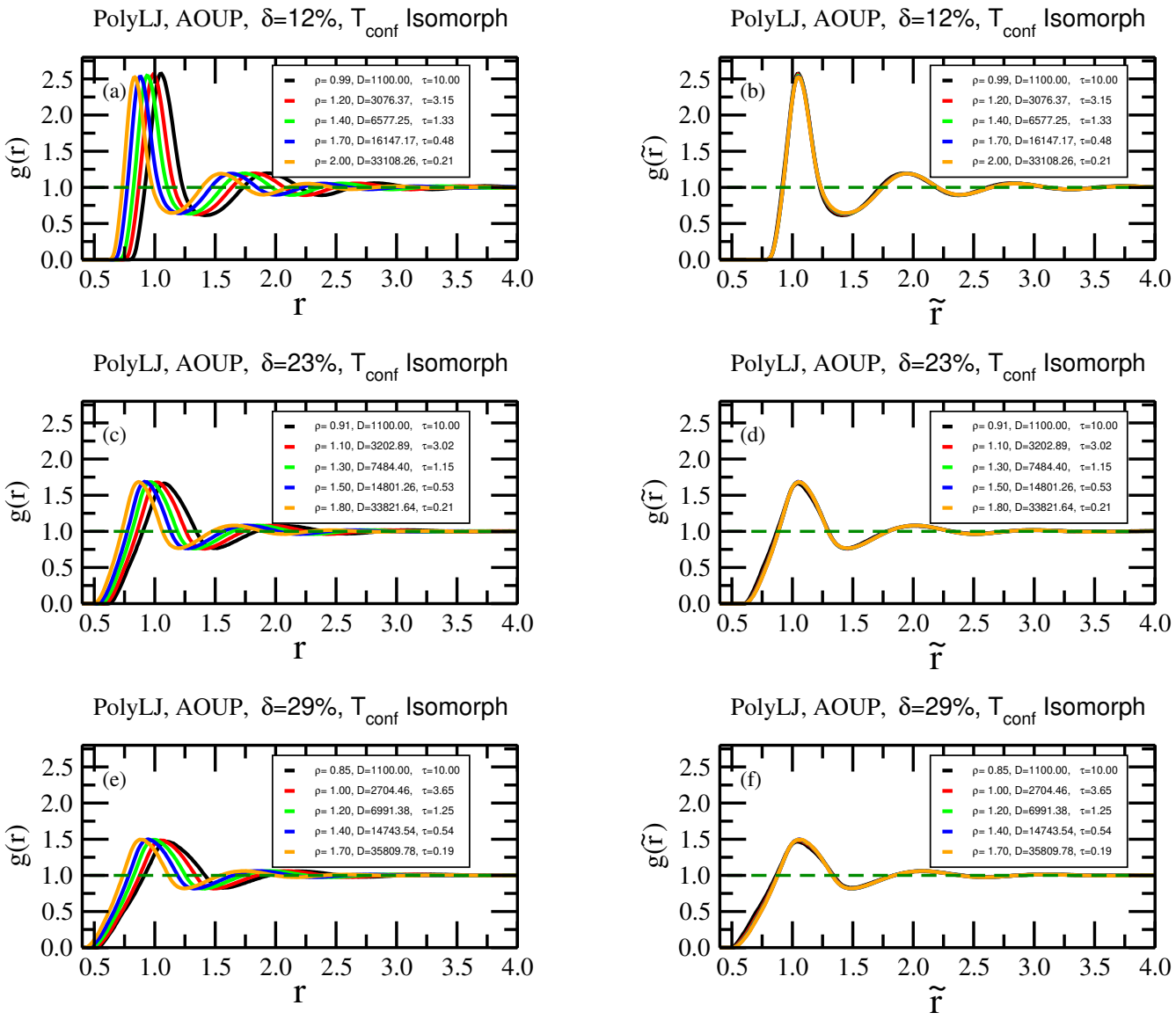

FIG. 2. Structure probed along $T_{\rm conf}$-generated active-matter isomorphs. (a), (c), and (e) show the average RDFs for polydispersity $\delta = 12\%$, 23%, and 29%, respectively, while (b), (d), and (f) show the same data as functions of the reduced pair distance $\tilde{r}$. In all three cases we see a good collapse of the reduced-unit RDF along the active-matter isomorphs.

Figure 3 shows analogous data for the MSD plotted in the same way with the left column giving the MSD as a function of time and the right column giving the same data in reduced units. There is a good data collapse with, however, a somewhat faster motion at the higher densities.

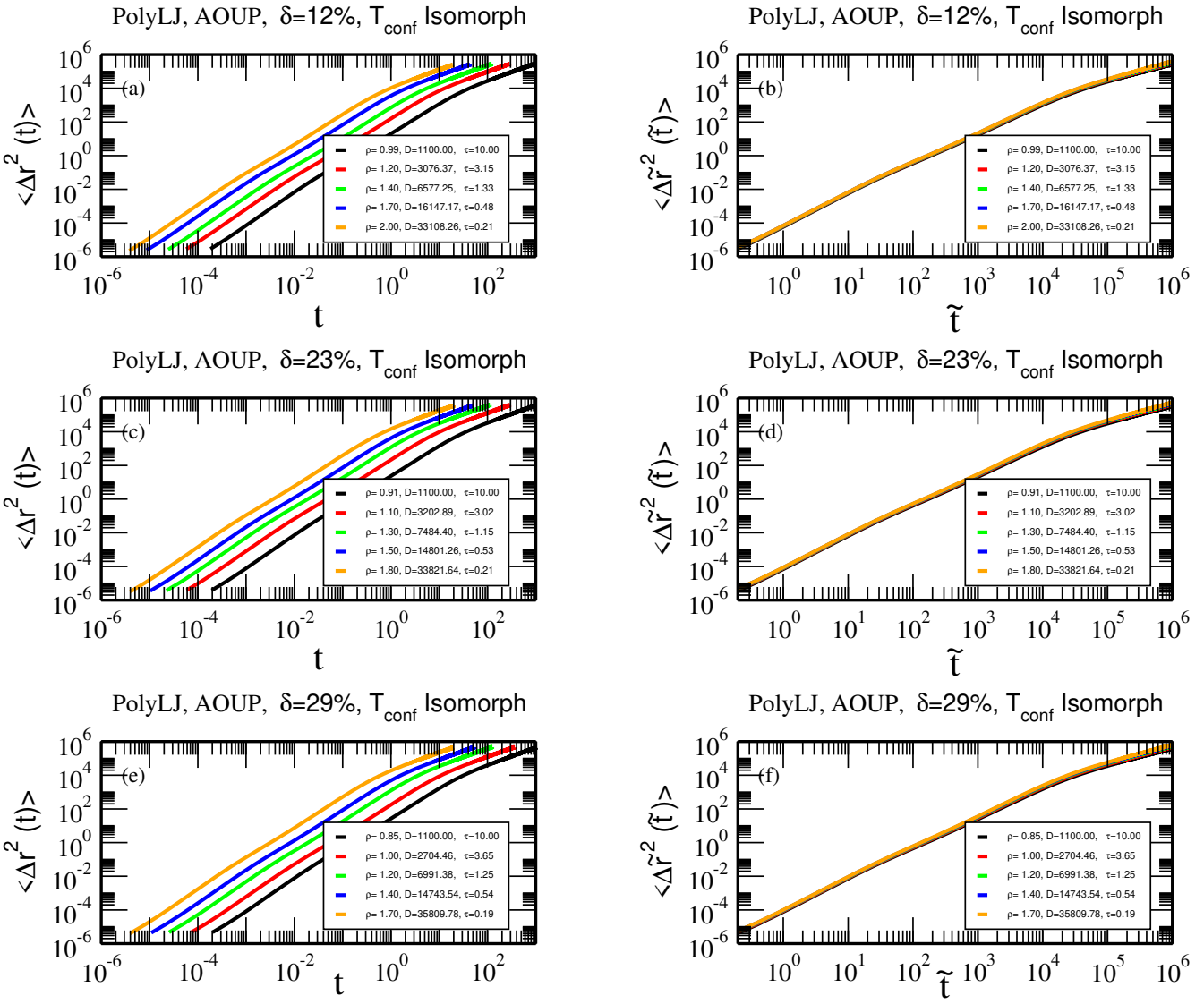

FIG. 3. Dynamics probed along $T_{\rm conf}$-generated active-matter isomorphs. (a), (c), and (e) show the MSDs for polydispersity $\delta = 12\%$, 23%, and 29%, respectively, as functions of time, while (b), (d), and (f) show the same data as functions of the reduced time $\tilde{t}$. There is a good, though not perfect, collapse of the reduced-unit MSD along the active-matter isomorphs.

V. COMPARING TO DIRECT-ISOMORPH-CHECK GENERATED ISOMORPHS

Above we demonstrated good invariance of the structure and dynamics along active-matter isomorphs generated by the $T_{\rm conf}$ method [26]. That method is easy to use and efficient because it requires just a single steady-state configuration at the reference state point in order to trace out the corresponding active-matter isomorph in the relevant phase diagram, *in casu* the (ρ, D, τ) diagram of the AOUP model. An alternative method for tracing out active-matter isomorphs is the analytical "direct isomorph-check" (DIC) method, which in Appendix A of Ref. 26 was shown to result in somewhat better isomorph-invariance of the dynamics for the AOUP Kob-Andersen binary LJ model.

Consider first a standard passive Newtonian systems involving LJ pair interactions of any kind, i.e., single-component, binary, or polydisperse systems, defined by some mixing rule that may or may not be the presently used Lorentz-Berthelot rule. For such a system the analytical DIC recipe for tracing out a standard equilibrium Newtonian isomorph [34, 35] is

$$\frac{h(\rho)}{T} \;=\; \text{Const.} \tag{5}$$

Here $h(\rho)$ is the following function of density [34, 35]

$$h(\rho) \;=\; \left(\frac{\gamma_0}{2}-1\right)\left(\frac{\rho}{\rho_0}\right)^4 - \left(\frac{\gamma_0}{2}-2\right)\left(\frac{\rho}{\rho_0}\right)^2 \tag{6}$$

in which ρ_0 is the reference-state-point density and γ_0 is the density-scaling exponent at the reference state point, which can be determined numerically by means of (where ΔW and ΔU are the deviations from the equilibrium values of virial and potential energy, respectively, and angular brackets denote NVT equilibrium values [25, 36]),

$$\gamma_0 \;=\; \frac{\langle \Delta U \Delta W\rangle}{\langle (\Delta U)^2\rangle}\,. \tag{7}$$

The systemic temperature $T_{\rm s}(\mathbf{R})$ is defined as the temperature of the corresponding thermal-equilibrium Newtonian system at the state point with the density of $\mathbf{R}$ and with average potential energy $U(\mathbf{R})$ [37]. In the thermodynamic limit of any system (passive or active, equilibrium or non-equilibrium) fluctuations in $T_{\rm s}(\mathbf{R})$ go to zero implying that at one has at any time a well-defined systemic temperature $T_{\rm s}$. For, e.g., a driven passive or an active-matter system, a "systemic isomorph" is defined as a curve in the $(\rho, T_{\rm s})$ phase diagram identical to an isomorph in the standard equilibrium Newtonian (ρ, T) phase diagram [37]. Thus in the analytical DIC, the systemic-temperature's variation with density is given by

$$\frac{h(\rho)}{T_{\rm s}(\rho)} \;=\; \text{Const.}\,, \tag{8}$$

i.e., $T_{\rm s}(\rho) \propto h(\rho)$. The analytical DIC method for generating an active-matter isomorph of the AOUP model is arrived at by replacing the configurational temperature in Eq. (3) by the systemic temperature $T_{\rm s}$ (justified in Ref. 26). Via Eq. (8) this leads to

$$\begin{aligned} D(\rho) \;&=\; D_0\,\frac{h(\rho)}{h(\rho_0)}\,,\\ \tau(\rho) \;&=\; \tau_0\left(\frac{\rho_0}{\rho}\right)^{2/3}\frac{h(\rho_0)}{h(\rho)}\,. \end{aligned} \tag{9}$$

Table II reports the systemic temperatures at the reference state points of the three polydispersities studied. As mentioned, the reference densities were chosen to have the same virial; we see that they also have almost the same systemic temperature.

ρ_0	δ	T_s	$\langle U\rangle$
0.990	12%	0.96	−4.455
0.905	23%	0.98	−4.447
0.850	29%	1.00	−4.321

TABLE II. Systemic temperature $T_{\rm s}$ and average potential energy $\langle U\rangle$ at the reference densities ρ_0 of the three polydisperse systems studied. In all three cases the values of the AOUP parameters at the reference densities are $D = 1100$ and $\tau = 10$.

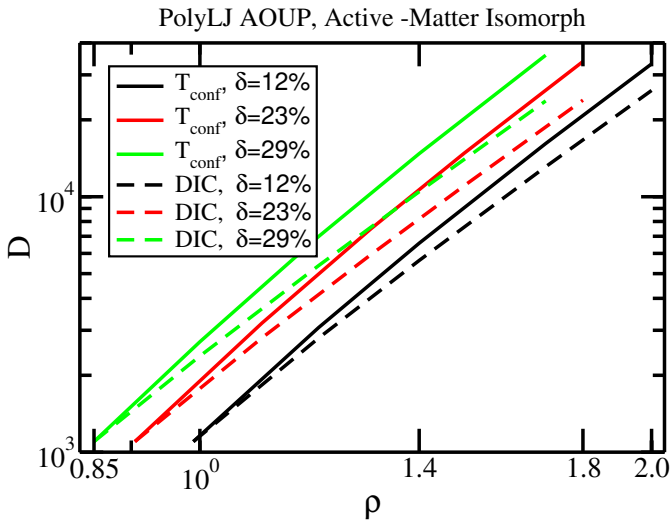

FIG. 4. Active-matter isomorphs of the polydispersities $\delta = 12\%$, 23%, and 29%, generated from the reference state points by two different methods, the $T_{\rm conf}$ method of Sec. III and the analytical direct-isomorph-check (DIC) method. The isomorphs are visibly different.

Fig. 4 shows the active-matter isomorph obtained from the $T_{\rm conf}$ method (full curves) and the analytical DIC method (dashed curves), starting at reference state point $(\rho, D, \tau) = (\rho_0, 1100, 10)$ in which the reference density is 0.99, 0.91, and 0.85, respectively, for polydispersity $\delta = 12\%$, 23%, and 29%. The two methods for generating isomorphs result in visibly different curves; there is more than 50% difference in D and τ at the largest density in the 29% polydispersity case (green curves). How different are these active-matter isomorphs when it comes to average RDF and MSD data collapse? The RDF case is investigated in Fig. 5, which shows that the structure is somewhat more invariant along the $T_{\rm conf}$-generated active-matter isomorphs than along the DIC-generated isomorphs.

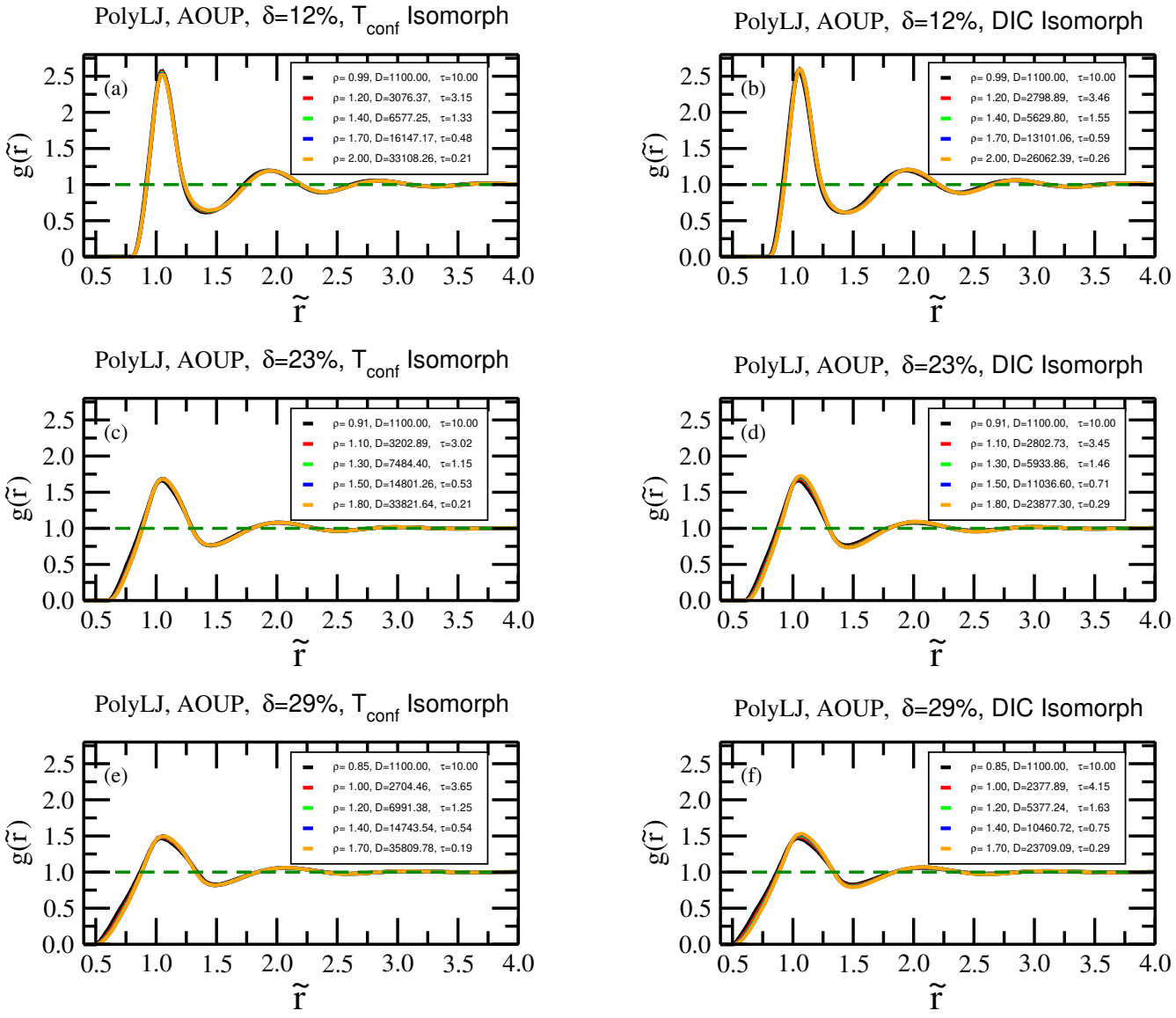

FIG. 5. Comparing the degree of structural invariance along $T_{\rm conf}$-generated and DIC-generated active-matter isomorphs. (a), (c), and (e) show the reduced-unit average RDFs for polydispersity $\delta = 12\%$, 23%, and 29%, along the $T_{\rm conf}$-generated isomorphs, while (b), (d), and (f) show the corresponding reduced-unit average RDFs along the DIC-generated isomorphs. There is a somewhat better data collapse along the $T_{\rm conf}$-generated isomorphs.

Figure 6 reports for the MSD. Here we reach the opposite conclusion: the DIC method results in a better data collapse than the $T_{\rm conf}$ method. The same conclusion was reached for the binary Kob-Andersen AOUP model in Ref. 26 (that did not investigate the average RDF).

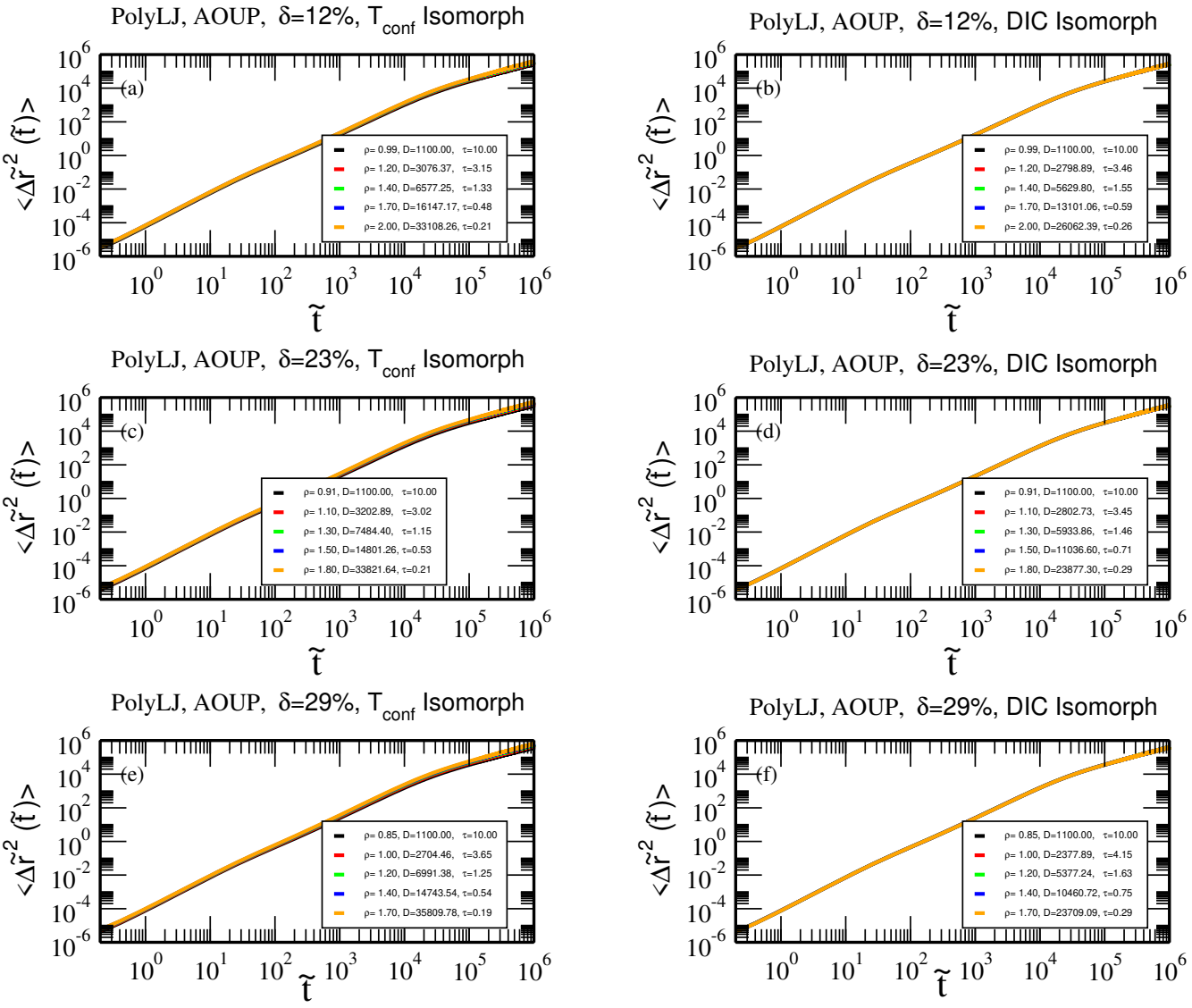

FIG. 6. Comparing the degree of invariance of the dynamics along the $T_{\rm conf}$-generated and DIC-generated active-matter isomorphs. (a), (c), and (e) show the reduced-unit MSDs for polydispersity $\delta = 12\%$, 23%, and 29%, along the $T_{\rm conf}$-generated isomorphs, while (b), (d), and (f) show the corresponding reduced-unit MSDs along the DIC-generated isomorphs. There is a better data collapse along the DIC-generated isomorphs.

VI. ROLE OF SMALLEST AND LARGEST PARTICLES

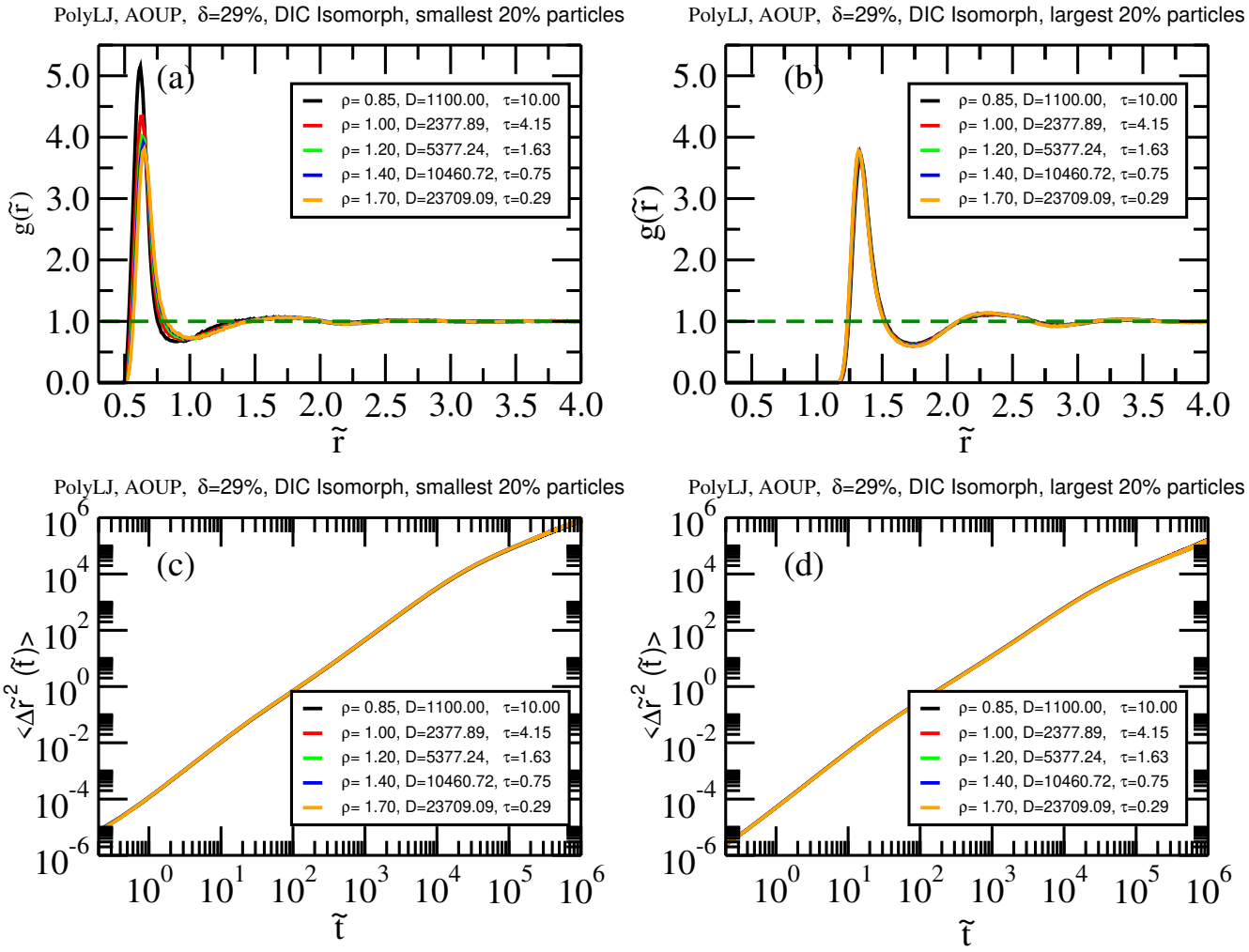

FIG. 7. Comparing the degree of invariance of the structure and dynamics of the 20% smallest and largest particles, along the DIC-generated active-matter isomorphs for the $\delta = 29\%$ polydispersity case. (a) and (c) show the reduced-unit RDFs. The invariance of the largest 20% particle RDF is much better than the small-particle RDF. For the MSD, however, both cases are isomorph invariant to a good approximation.

We have seen that the structure is slightly less invariant along the DIC-generated isomorph than along the $T_{\rm conf}$ isomorph (Fig. 5). To briefly investigate a possible cause of this we studied the structure and dynamics along the DIC isomorph of the 20% smallest and the 20% largest particles. The RDF is here defined by limiting the central particle to being either among the smallest or the largest 20% and then counting all neighboring particles of the same kind; the MSD represents the mean-square displacement averaged over only the smallest and largest particles, respectively.

The result of this analysis of the 29% polydispersity simulation data is given in Fig. 7. Interestingly, the structure around the smallest particles is not DIC-isomorph invariant, while that of the largest is. In contrast, for the dynamics both cases are DIC-isomorph invariant to a good approximation, which is interesting because the data show that smallest particles move faster than the largest ones. In support of a conjecture that the fact that the smallest particles' structure is less invariant explains the lack of isomorph invariance of the overall RDF, we note that in both Fig. 5(f) and in Fig. 7(a) the most pronounced structure is seen at the highest density.

VII. SUMMARY AND OUTLOOK

We have shown that the uniform-distribution size-polydisperse LJ AOUP model has active-matter isomorphs for the polydispersities $\delta = 12\%$, 23%, and 29%. This demonstrates the robustness of the active-matter-isomorph concept, which for passive systems applies whenever the potential-energy function obeys the hidden-scale-invariance condition discussed in Refs. 38 and 39. The existence of isomorphs means that the dimension of the AOUP phase diagram is effectively reduced from three to two since lines exist in the (ρ, D, τ) phase diagram along which the reduced-unit structure and dynamics are invariant to a good approximation. From a practical perspective, this fact makes it easier to quickly get an overview of the AOUP model's phase diagram.

More work is needed to clarify how polydispersity relates to the existence of active-matter isomorphs in general. As regards the AOUP model, it would be interesting to investigate whether the introduction of energy polydispersity affects the existence of isomorphs. More generally, other models like the active Brownian particle model with a potential-energy function that obeys hidden scale invariance should be investigated in polydisperse versions in order to illuminate the robustness of the active-matter-isomorph concept.

ACKNOWLEDGMENTS

This work was supported by the VILLUM Foundation's *Matter* grant (16515).

[1] R. Mandal, P. J. Bhuyan, P. Chaudhuri, C. Dasgupta, and M. Rao, "Extreme active matter at high densities," Nat. Comm. **11**, 2581 (2020).
[2] J. O'Byrne, Y. Kafri, J. Tailleur, and F. van Wijland, "Time irreversibility in active matter, from micro to macro," Nat. Rev. Phys. **4**, 167–183 (2022).
[3] T. E. Angelini, E. Hannezo, X. Trepat, M. Marquez, J. J. Fredberg, and D. A. Weitz, "Glass-like dynamics of collective cell migration," Proc. Natl. Acad. Sci. (USA) **108**, 4714–4719 (2011).
[4] M. C. Marchetti, J. F. Joanny, S. Ramaswamy, T. B. Liverpool, J. Prost, M. Rao, and R. A. Simha, "Hydrodynamics of soft active matter," Rev. Mod. Phys. **85**, 1143–1189 (2013).
[5] C. Bechinger, R. Di Leonardo, H. Löwen, C. Reichhardt, G. Volpe, and G. Volpe, "Active particles in complex and crowded environments," Rev. Mod. Phys. **88**, 045006 (2016).
[6] S. Ramaswamy, "Active matter," J. Stat. Mech. , 054002 (2017).
[7] D. Saintillan, "Rheology of active fluids," Annu. Rev. Fluid Mech. **50**, 563–592 (2018).
[8] M. Das, C. F. Schmidt, and M. Murrell, "Introduction to active matter," Soft Matter **16**, 7185–7190 (2020).
[9] M. R. Shaebani, A. Wysocki, R. G. Winkler, G. Gompper, and H. Rieger, "Computational models for active matter," Nat. Rev. Phys. **2**, 181–199 (2021).
[10] M. J. Bowick, N. Fakhri, C. M. Marchetti, and S. Ramaswamy, "Symmetry, thermodynamics, and topology in active matter," Phys. Rev. X **12**, 010501 (2022).
[11] A. Marruzzo, W. Schirmacher, A. Fratalocchi, and G. Ruocco, "Heterogeneous shear elasticity of glasses: the origin of the boson peak," Scientific Reports **3**, 1407 (2013).
[12] S. C. Takatori and J. F. Brady, "Towards a thermodynamics of active matter," Phys. Rev. E **91**, 032117 (2015).
[13] T. F. F. Farage, P. Krinninger, and J. M. Brader, "Effective interactions in active Brownian suspensions," Phys. Rev. E **91**, 042310 (2015).
[14] C. Maggi, U. M. B. Marconi, N. Gnan, and R. Di Leonardo, "Multidimensional stationary probability distribution for interacting active particles," Sci. Rep. **5**, 10742 (2015).
[15] G. Szamel, E. Flenner, and L. Berthier, "Glassy dynamics of athermal self-propelled particles: Computer simulations and a nonequilibrium microscopic theory," Phys. Rev. E **91**, 062304 (2015).
[16] E. Fodor, C. Nardini, M. E. Cates, J. Tailleur, P. Visco, and F. van Wijland, "How far from equilibrium is active matter?" Phys. Rev. Lett. **117**, 038103 (2016).
[17] R. Ni, M. A. C. Stuart, and P. G. Bolhuis, "Tunable long range forces mediated by self-propelled colloidal hard spheres," Phys. Rev. Lett. **114**, 018302 (2015).
[18] S. Henkes, K. Kostanjevec, J. M. Collinson, R. Sknepnek, and E. Bertin, "Dense active matter model of motion patterns in confluent cell monolayers," Nat. Comm. **11**, 1405 (2020).
[19] S. Kumar, J. P. Singh, D. Giri, and S. Mishra, "Effect of polydispersity on the dynamics of active Brownian particles," Phys. Rev. E **104**, 024601 (2021).
[20] G. Szamel and E. Flenner, "Long-ranged velocity correlations in dense systems of self-propelled particles," Europhys. Lett. **133**, 60002 (2021).
[21] Andrea Ninarello, Ludovic Berthier, and Daniele Coslovich, "Models and algorithms for the next generation of glass transition studies," Phys. Rev. X **7**, 021039 (2017).

[22] S. E. Abraham, S. M. Bhattacharrya, and B. Bagchi, "Energy landscape, antiplasticization, and polydispersity induced crossover of heterogeneity in supercooled polydisperse liquids," Phys. Rev. Lett. **100**, 167801 (2008).

[23] E. Zaccarelli, S. M. Liddle, and W. C. K. Poon, "On polydispersity and the hard sphere glass transition," Soft Matter **11**, 324 (2015).

[24] I. Pihlajamaa, C. C. L. Laudicina, and L. M.C. Janssen, "Polydispersity modifies relaxation mechanisms in glassy liquids," arXiv , 2302.09549 (2023).

[25] N. Gnan, T. B. Schrøder, U. R. Pedersen, N. P. Bailey, and J. C. Dyre, "Pressure-energy correlations in liquids. IV. "Isomorphs" in liquid phase diagrams," J. Chem. Phys. **131**, 234504 (2009).

[26] S. Saw, L. Costigliola, and J. C. Dyre, "Configurational temperature in active matter. I. Lines of invariant physics in the phase diagram of the Ornstein-Uhlenbeck model," Phys. Rev. E **107**, 024609 (2023).

[27] S. Saw, L. Costigliola, and J. C. Dyre, "Configurational temperature in active matter. II. Quantifying the deviation from thermal equilibrium," Phys. Rev. E **107**, 024610 (2023).

[28] T. S. Ingebrigtsen, T. B. Schrøder, and J. C. Dyre, "Hidden scale invariance in polydisperse mixtures of exponential repulsive particles," J. Phys. Chem. B **125**, 317–327 (2021).

[29] S. Toxvaerd and J. C. Dyre, "Communication: Shifted forces in molecular dynamics," J. Chem. Phys. **134**, 081102 (2011).

[30] N. P. Bailey, T. S. Ingebrigtsen, J. S. Hansen, A. A. Veldhorst, L. Bøhling, C. A. Lemarchand, A. E. Olsen, A. K. Bacher, L. Costigliola, U. R. Pedersen, H. Larsen, J. C. Dyre, and T. B. Schrøder, "RUMD: A general purpose molecular dynamics package optimized to utilize GPU hardware down to a few thousand particles," Scipost Phys. **3**, 038 (2017).

[31] L. D. Landau and E. M. Lifshitz, *Statistical Physics* [Eq. (33.14)] (Pergamon, Oxford, 1958).

[32] H. H. Rugh, "Dynamical approach to temperature," Phys. Rev. Lett. **78**, 772–774 (1997).

[33] J. G. Powles, G. Rickayzen, and D. M. Heyes, "Temperatures: old, new and middle aged," Mol. Phys. **103**, 1361–1373 (2005).

[34] L. Bøhling, T. S. Ingebrigtsen, A. Grzybowski, M. Paluch, J. C. Dyre, and T. B. Schrøder, "Scaling of viscous dynamics in simple liquids: Theory, simulation and experiment," New J. Phys. **14**, 113035 (2012).

[35] T. S. Ingebrigtsen, L. Bøhling, T. B. Schrøder, and J. C. Dyre, "Thermodynamics of condensed matter with strong pressure-energy correlations," J. Chem. Phys. **136**, 061102 (2012).

[36] N. P. Bailey, U. R. Pedersen, N. Gnan, T. B. Schrøder, and J. C. Dyre, "Pressure-energy correlations in liquids. I. Results from computer simulations," J. Chem. Phys. **129**, 184507 (2008).

[37] J. C. Dyre, "Isomorph theory beyond thermal equilibrium," J. Chem. Phys. **153**, 134502 (2020).

[38] T. B. Schrøder and J. C. Dyre, "Simplicity of condensed matter at its core: Generic definition of a Roskilde-simple system," J. Chem. Phys. **141**, 204502 (2014).

[39] J. C. Dyre, "Perspective: Excess-entropy scaling," J. Chem. Phys. **149**, 210901 (2018).